Applied Catalysis B: Environment and Energy 350 (2024) 123917

Contents lists available at ScienceDirect

Applied Catalysis B: Environment and Energy

journal homepage: www.elsevier.com/locate/apcatb

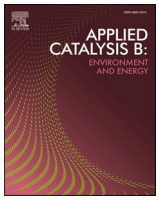

Synergetic effect for highly efficient light-driven CO_2 reduction by CH_4 on Co/Mg-$CoAl_2O_4$ promoted by a photoactivation

Zhengyan Cui, Qianqian Hu, Yuanzhi Li *, Jichun Wu, Xiaocui Yu, Huamin Cao, Lei Ji, Mengqi Zhong, Zhi Chen

State Key Laboratory of Silicate Materials for Architectures, Wuhan University of Technology, 122 Luoshi Road, Wuhan 430070, PR China

ARTICLE INFO

Keywords:
CO_2 reduction
Photothermocatalytic
Co nanoparticles
Mg-doped
Photoactivation

ABSTRACT

The utilization of photothermocatalytic dry reforming of methane is shown to be an up-and-coming technology. However, reaching high fuel productivity at a comparatively low light intensity and effectively suppressing the side reactions of coking in the DRM process are still two tough difficulties. Under focused UV–vis–IR irradiation at a relatively low light intensity of 80.5 kW m^{-2}, a nanostructure of Co/Mg-$CoAl_2O_4$ possesses excellent photothermocatalytic activity and a light-to-fuel efficiency of 34.2 % and a low carbon deposition rate compared to its reference catalyst without Mg^{2+} doping (Co/$CoAl_2O_4$). The improved photothermocatalytic activity and coking resistance of Co/Mg-$CoAl_2O_4$ mainly comes from the synergetic effect, including Mg^{2+} doping, the active lattice oxygen in $CoAl_2O_4$ also participating in the oxidation of carbon species, and strong light absorption properties of the Mg-$CoAl_2O_4$. The photoactivation promotes DRM on Co nanoparticles while significantly facilitates the C* oxidation by strongly adsorbed CO_2 on doped Mg^{2+}.

1. Introduction

Increasing demand for fossil fuels has caused energy shortages and massive CO_2 emissions leading to global environmental issues [1,2]. Dry reforming of methane (DRM, $CO_2 + CH_4 = 2CO_2 + H_2$, ΔH_{298} = 247 kJ mol^{-1}) is causing widespread concern owing to the reduction of two greenhouse gases and the production of syngas in its reaction process, which further creates high-valued chemical products by the Fischer-Tropsch process [3–6]. However, due to the thermodynamics of DRM reaction (ΔH_{298} = 247 kJ mol^{-1}), traditional thermocatalytic DRM usually needs a high reaction temperature of over 750 °C [7–12], bringing an increase in energy consumption. The catalyst is prone to deactivation caused by sintering under such harsh reaction conditions, seriously affecting the catalytic durability of the catalyst in DRM. Although using solar energy to drive photocatalysis to produce syngas has been used as a promising alternative and widely studied [13–28], the undesirable production fuel rates (r_{fuel}) and light-to-fuel efficiency (η) resulting from fast recombination of photo-induced charge carriers and low utilization rate of light absorption are difficult to overcome and limit the meet of application in modern industry.

A strategy of photothermocatalytic DRM, combining the high catalytic activity of thermal catalysis with the competitive energy cost of photocatalysis, has aroused great attention [29–54]. Noble metal catalysts (e.g., Pd, Pt, Ru, Rh, etc.) demonstrated great catalytic performance, but their high cost and scarce reserves have restricted their large-scale applications [29,30]. The accessible and inexpensive Co-based catalysts become an ideal alternative. However, two challenges in recent photothermocatalytic DRM need to be tackled immediately. For one thing, a strong intensity of focused light higher than 192 kW m^{-2} is a necessary demand for achieving large fuel yields and light-to-fuel efficiency in recent researches [30–37,39,40,42,43]. This requires expensive focused light equipment, which increases the cost and is hard to implement in practical conditions. For another thing, Co-based catalysts are more susceptible to coke due to thermodynamically unavoidable side reactions [37]. The rapid deactivation and poor anti-coking performance block the further practical application of Co-based catalysts.

In this work, we fabricate a nanostructure consisting of Co nanoparticles loaded on Mg-doped $CoAl_2O_4$ (Co/Mg-$CoAl_2O_4$). Co/Mg-$CoAl_2O_4$ exhibits extremely high r_{H2} and r_{CO} and a superb η at a lower intensity of 80.5 kW m^{-2}. It possesses excellent durability after a 60 h photothermocatalytic DRM reaction and has good anti-coking performance. Co/Mg-$CoAl_2O_4$ has a low carbon deposition rate, which is the 0.038 times that of its reference sample (Co/$CoAl_2O_4$). The synergetic

* Corresponding author.
E-mail address: liyuanzhi@whut.edu.cn (Y. Li).

https://doi.org/10.1016/j.apcatb.2024.123917
Received 16 January 2024; Received in revised form 27 February 2024; Accepted 3 March 2024
Available online 5 March 2024

effect between Mg^{2+} doping, active lattice oxygen and strong light absorption of Mg-$CoAl_2O_4$ significantly promote the photothermocatalytic activity and coking resistance on Co/Mg-$CoAl_2O_4$. Mg^{2+} doping improves the CO_2 adsorption capacity of $CoAl_2O_4$ and the strongly absorbed CO_2 on doped Mg^{2+} accelerates the oxidation of carbon species (C*). The lattice oxygens in the Co–O binds of $CoAl_2O_4$ are also engages in the C* oxidation, resulting in improves coking resistance. And the strong light absorption of Mg-$CoAl_2O_4$ strengthens the light absorption capacity of Co/Mg-$CoAl_2O_4$. The synergetic effect of these factors contributes to the superb photothermocatalytic performance of Co/Mg-$CoAl_2O_4$ even at a lower light intensity. Another reason for the high photothermocatalytic activity of Co/Mg-$CoAl_2O_4$ can be achieved at lower light intensity is photoactivation, which significantly reduces activation energy and promotes C* oxidation. The focused illumination further significantly facilitates the C* oxidation by strongly adsorbed CO_2 on doped Mg^{2+} greatly enhancing the photothermocatalytic activity. Upon a series of experiments, the synergetic effect of Mg^{2+} doping, the lattice oxygen in $CoAl_2O_4$ besides the strong light absorption of Mg-$CoAl_2O_4$ and the role of light were revealed.

2. Preparation

5.6307 g of $Al(NO_3)_3{\cdot}9H_2O$ and 0.2183 g of $Co(NO_3)_2{\cdot}6H_2O$ were dissolved in a beaker with 20 mL of deionized water, magnetically stirred for 20 min. 4.9654 g of citric acid monohydrate was dissolved in 20 mL of deionized water before being added to the above-mixed solution. Then, the mixed solution was magnetically stirred at 90 °C for 3 h to form the sol-gel solution. The obtained gel was dried at 120 °C for 12 h and calcined at 600 °C for 4 h. The acquired powder was marked as $CoAl_2O_4$.

0.0715 g of $Co(NO_3)_2{\cdot}6H_2O$, 0.0307 g of $Mg(NO_3)_2{\cdot}6H_2O$, and 5 mL of deionized water were added together to form a mixed solution. Then, the mixed solution and 0.1450 g of $CoAl_2O_4$ were added to an evaporating dish. The evaporating dish was placed on a heating plate of 180 °C and the mixed sample was ground to dry. Subsequently, resultant sample was calcined at 500 °C for 3 h. 0.0500 g of powder sample was reduced in a 5 vol % H_2/Ar stream (30 mL min^{-1}) at 750 °C for 1 h. The obtained sample was denoted as Co/Mg-$CoAl_2O_4$.

Co/$CoAl_2O_4$ sample was fabricated following the same process as Co/Mg-$CoAl_2O_4$ except for not adding $Mg(NO_3)_2{\cdot}6H_2O$. Mg-$CoAl_2O_4$ sample was prepared in the same procedure as Co/Mg-$CoAl_2O_4$ except for not adding $Co(NO_3)_2{\cdot}6H_2O$.

3. Results and discussion

3.1. Characterization

The preparation of Co nanoparticles loaded on Mg-doped $CoAl_2O_4$ (Co/Mg-$CoAl_2O_4$) was obtained by wet impregnation mixing $Co(NO_3)_2$ and $Mg(NO_3)_2$ solutions with $CoAl_2O_4$ samples. Followed by calcination at 500 °C, and pre-reduced at 750 °C with a stream of 5 vol % H_2/Ar for 1 h. For comparison, Co nanoparticles supported on $CoAl_2O_4$ (Co/

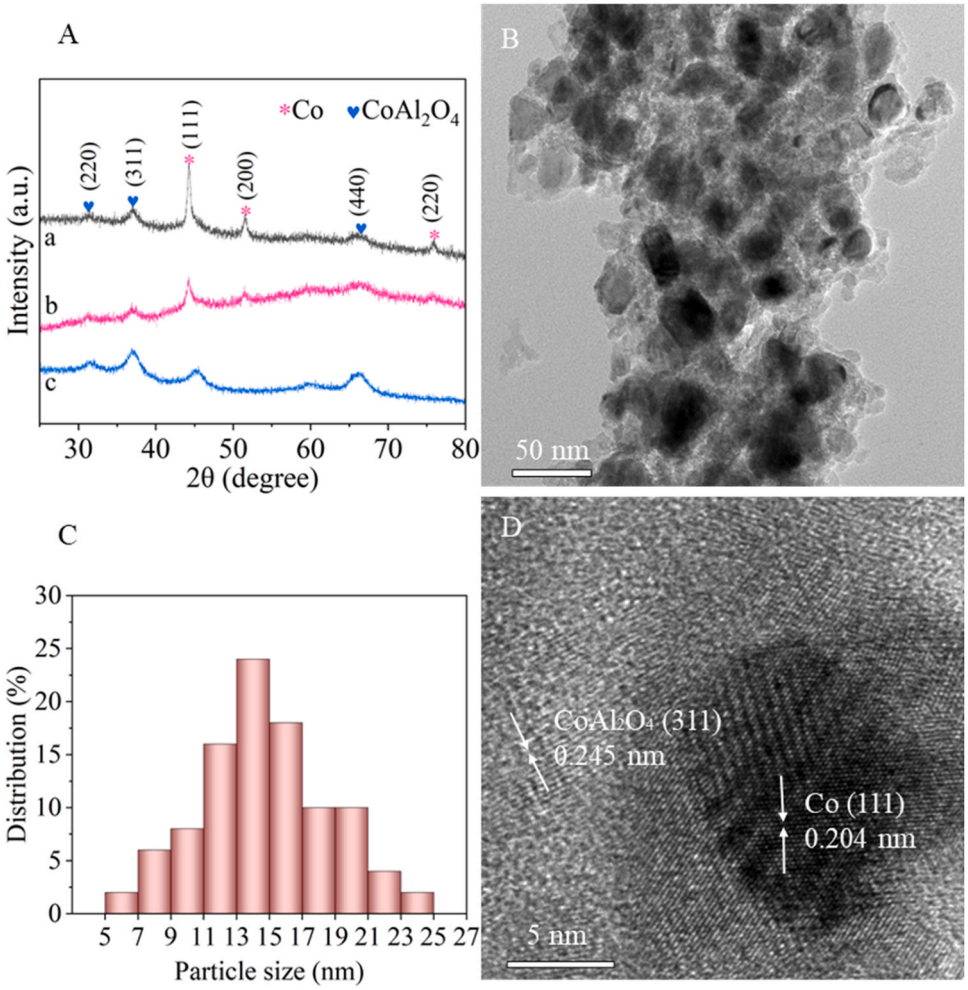

Fig. 1. XRD patterns (A) of Co/Mg-$CoAl_2O_4$ (a), Co/$CoAl_2O_4$ (b), Mg-$CoAl_2O_4$ (c), TEM image (B), the size distribution of Co nanoparticles in Co/Mg-$CoAl_2O_4$ (C) and HRTEM image (D) of Co/Mg-$CoAl_2O_4$.

$CoAl_2O_4$) was fabricated using the same method apart from not adding $Mg(NO_3)_2$ solution. ICP-OES results suggest that the mole ratios of Co/Al for Co/Mg-$CoAl_2O_4$, Co/$CoAl_2O_4$, and Mg-$CoAl_2O_4$ are 0.1570, 0.1591, and 0.0338, respectively. The mole ratios of Mg/Al for Co/Mg-$CoAl_2O_4$ and Mg-$CoAl_2O_4$ are 0.0523 and 0.0365, respectively (SI. Formula 1).

XRD patterns of Co/Mg-$CoAl_2O_4$, Co/$CoAl_2O_4$, and Mg-$CoAl_2O_4$ are shown in Fig. 1A. The peaks at 31.23°, 36.79°, 44.74°, 55.57° and 59.27° are attributed to $CoAl_2O_4$ (PDF 70–0753). Characteristic diffraction peaks at 44.22°, 51.52°, and 75.85° of metallic Co (PDF 15–0806) are observed in Co/Mg-$CoAl_2O_4$, Co/$CoAl_2O_4$. The peaks of Mg and its compounds are not detected in the XRD patterns, which is probably due to Mg is doped in $CoAl_2O_4$ lattice or the high dispersion or the small crystal size of MgO in the sample. By Scherrer's formula ($L = 0.89\lambda/\beta\cos\theta$), the average particle sizes of metallic Co nanoparticles at (111) facet ($2\theta = 44.22°$) are estimated to be 14.7 and 11.4 nm in Co/Mg-$CoAl_2O_4$ and Co/$CoAl_2O_4$, respectively. Further, the fresh samples of Co/Mg-$CoAl_2O_4$ and Co/$CoAl_2O_4$ were characterized by TEM. As revealed by TEM images, all the catalysts display a nanosheet structure (Fig. 1B and Figure S1). We measured the Co nanoparticle size for Co/Mg-$CoAl_2O_4$ and Co/$CoAl_2O_4$ made particle distribution map (Fig. 1D and S1C). The main particle size of Co nanoparticles is 13–15 nm and 11–13 nm, respectively, which is basically consistent with the XRD results. The Co nanoparticles of Co/Mg-$CoAl_2O_4$ and Co/Mg-$CoAl_2O_4$ are more dispersed and unevenly distributed. In HRTEM images of Co/Mg-$CoAl_2O_4$ and Co/$CoAl_2O_4$, the lattice spacing of 0.204 nm matching with metallic Co nanoparticles (111) facet, and the lattice spacing of 0.245 nm matching with $CoAl_2O_4$ (311) facet are observed (Fig. 1D and Figure S1). There is no detectable crystal lattice of MgO in the HRTEM image of Co/Mg-$CoAl_2O_4$. Element mapping of Co/Mg-$CoAl_2O_4$ confirms that metallic Co nanoparticles are uniformly distributed, and Mg is well dispersed on $CoAl_2O_4$ (Fig. 2). This is consistent with the XRD and HRTEM results. For Co/$CoAl_2O_4$, the element mapping shows that metallic Co nanoparticles are evenly supported on $CoAl_2O_4$ (Figure S2).

XPS was applied to detect the surface chemical components (Figure S3). Al and O elements in Co/Mg-$CoAl_2O_4$ and Co/$CoAl_2O_4$ exist as Al^{3+} and O^{2-}, respectively. Mg element in Co/Mg-$CoAl_2O_4$ exists as Mg^{2+}. The two strong peaks at 796.5 eV and 780.4 eV are identical to the binding energies of Co^{2+} $2p_{1/2}$ and Co^{2+} $2p_{3/2}$ of $CoAl_2O_4$, respectively. The peaks at 786.4 eV and 802.6 eV are attributed to the Co $2p_{3/2}$ and Co $2p_{1/2}$ satellite peaks of Co^{2+}. The peak at 777.9 eV belongs to the Co^0 $2p_{3/2}$ of metallic Co nanoparticles.

N_2 adsorption was further used to characterize the distribution of pore sizes and the specific surface area of catalysts (Figure S4). The BET-specific surface areas of Co/Mg-$CoAl_2O_4$, Co/$CoAl_2O_4$, and Mg-$CoAl_2O_4$ are 72.8, 45.1, and 91.5 $m^2\ g^{-1}$, respectively. The BJH adsorption pore volumes were 0.10, 0.08, and 0.13 $cm^3\ g^{-1}$, respectively.

3.2. Photothermocatalytic activity

The photothermocatalytic DRM on the samples under focused UV–vis–IR illumination by a 500 W Xe lamp at a light intensity of 80.5 kW m^{-2} with no external heating conditions was conducted. A feed stream of 29.2/29.8/41.0 vol % $CH_4/CO_2/Ar$ flowed steadily into the reaction system at 93.07 mL min^{-1} (SI, Experimental). The amount of catalyst used is 0.01 g. As can be seen from Fig. 3A and B, Mg-$CoAl_2O_4$ displays merely a little photothermocatalytic activity. The reaction rates

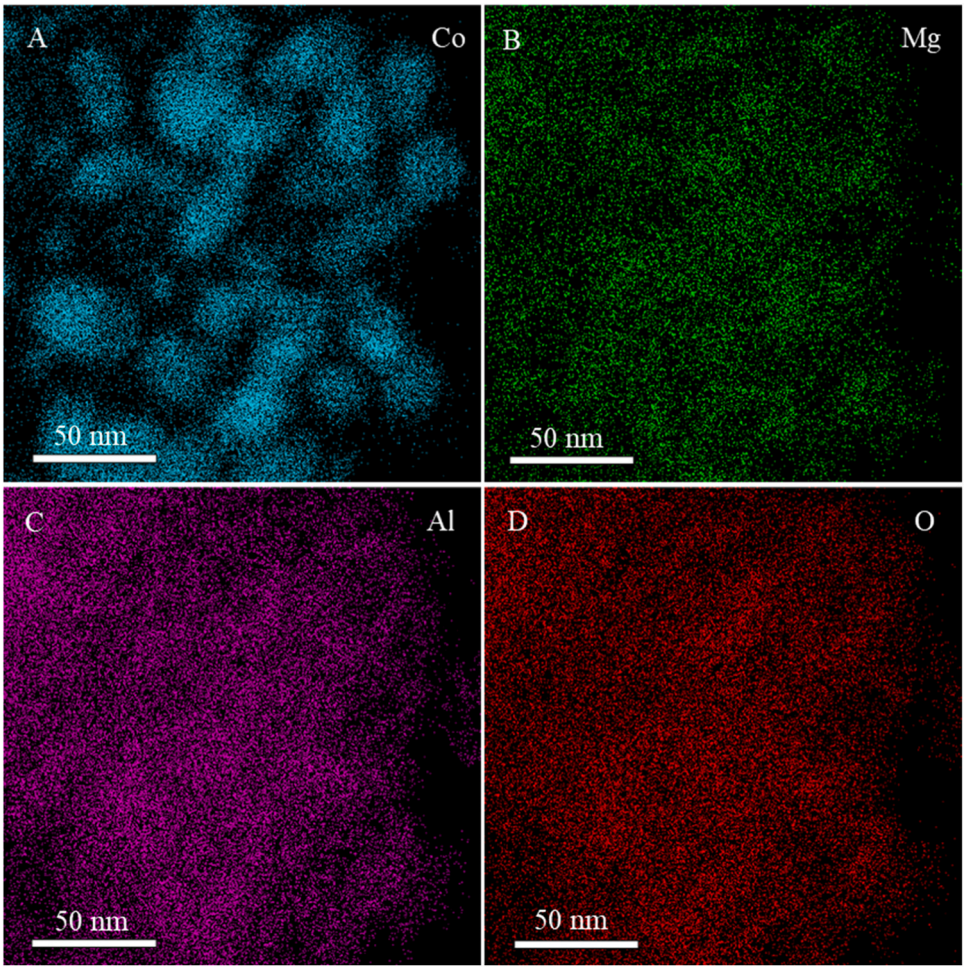

Fig. 2. The EDS mapping with the corresponding elements (A-D) of Co/Mg-$CoAl_2O_4$.

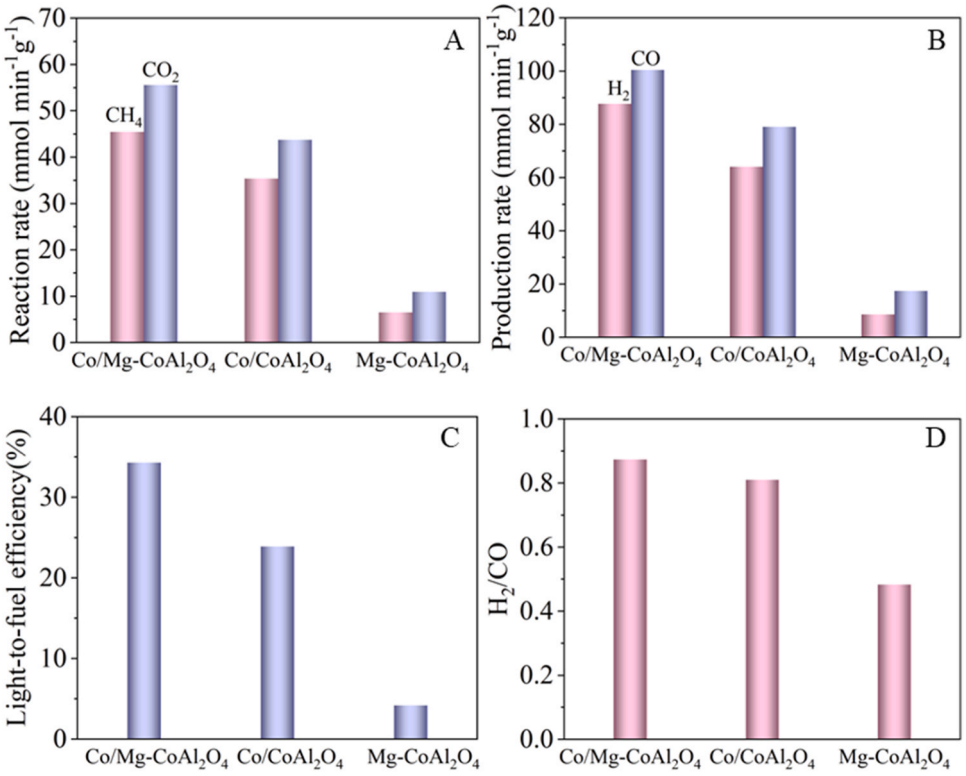

Fig. 3. The values of r_{CH4} and r_{CO2} (A), the values of r_{H2} and r_{CO} (B), the values of η (C), and H_2/CO (D) of Co/Mg-$CoAl_2O_4$, Co/$CoAl_2O_4$ and Mg-$CoAl_2O_4$ for photothermocatalytic DRM under focused UV–vis–IR irradiation.

of CO_2 (r_{CO2}) and CH_4 (r_{CH4}) of Mg-$CoAl_2O_4$ are 10.92 and 6.49 mmol min^{-1} g^{-1}, respectively. Its production rates of H_2 (r_{H2}) and CO (r_{CO}) are 8.58 and 17.37 mmol min^{-1} g^{-1}, respectively. Most strikingly, Co/Mg-$CoAl_2O_4$ shows exceedingly high photothermocatalytic activity, with fuel production values higher than those of the state-of-the-art of catalysts that react at high light intensity (Table S1). The r_{CH4} and r_{CO2} are 45.43 and 55.55 mmol min^{-1} g^{-1}, respectively. The r_{H2} and r_{CO} are 87.67 and 100.41 mmol min^{-1} g^{-1}, respectively. Since Mg-$CoAl_2O_4$ is almost inactive, the remarkable enhancement of the activity of Co/Mg-$CoAl_2O_4$ reveals that the main activity arises from the metallic Co nanoparticles. Compared to Co/Mg-$CoAl_2O_4$, Co/$CoAl_2O_4$ exhibits lower photothermocatalytic activity with r_{CH4} and r_{CO2} values of 35.38 and 43.72 mmol min^{-1} g^{-1}, respectively. And its r_{H2} and r_{CO} are 63.99 and 79.03 mmol min^{-1} g^{-1}, respectively. The turnover frequency (TOF) of H_2 for Co/Mg-$CoAl_2O_4$ and Co/$CoAl_2O_4$ is calculated as 744.11 and 257.04 min^{-1}, respectively (SI Formula 2) The TOF of Co/Mg-$CoAl_2O_4$ is 3 times higher than that of Co/$CoAl_2O_4$. The lower molar ratio of H_2 to CO than the stoichiometric ratio of DRM (1: 1) is caused by a side reaction of water-gas reversal ($H_2 + CO_2 = H_2O + CO$). The ratio of H_2 to CO in Co/Mg-$CoAl_2O_4$ is 0.87, which is higher than that on Co/$CoAl_2O_4$ (0.81) and Mg-$CoAl_2O_4$ (0.48) (Fig. 3D). This implies that Co/Mg-$CoAl_2O_4$ is the least affected by the side reaction. DRM is an intense endothermic reaction, and its intense endothermic property (ΔH_{298} = 247 kJ mol^{-1}) means that photothermocatalytic DRM on Co/Mg-$CoAl_2O_4$ driven solely by concentrated UV–vis–IR illumination can realize an efficient solar-fuel conversion.

Therefore, light-to-fuel efficiency (η) is obtained based on the formula below:

$$\eta = (\Delta_c H^0_{CO} \times r_{CO} + \Delta_c H^0_{H2} \times r_{H2} - \Delta_c H^0_{CH4} \times r_{CH4})/P_{illumination}$$

$\Delta_c H^0_{CO}$, $\Delta_c H^0_{H2}$, and $\Delta_c H^0_{CH4}$, are the standard combustion heats (298.15 K) of CO, H_2, and CH_4 as fuels, respectively (*Note*: $\Delta_c H^0_{CO2}$ is 0). $P_{illumination}$ is the illumination power.

Under focused UV–vis–IR radiation, the η value of Mg-$CoAl_2O_4$ is 4.25 %. The η value of Co/Mg-$CoAl_2O_4$ is the highest at 34.2 %, far surpassing the η value of Co/$CoAl_2O_4$ (23.8 %).

The activities of photothermocatalytic DRM on Co/Mg-$CoAl_2O_4$ under focused vis-IR irradiation at comparatively low light intensities were also performed. With focused light irradiation filtered by a 420 nm filter, Co/Mg-$CoAl_2O_4$ possesses high r_{CH4} and r_{CO2} values of 33.38 and 44.91 mmol min^{-1} g^{-1}, respectively (Fig. 4A). Its r_{H2} and r_{CO} values are 59.76 and 77.96 mmol min^{-1} g^{-1}, respectively (Fig. 4B), with a η of 29.5 % (Fig. 4C). Even with focused light irradiation filtered by a 690 nm filter, Co/Mg-$CoAl_2O_4$ still obtains good photothermocatalytic DRM activity (Figs. 4A and 4B) as well as a high η of 21.5 % (Fig. 4C).

3.3. Photothermocatalytic durability

The assessment of photothermocatalytic durability of catalysts is vital because it decides the large-scale practical applications of DRM. A significant challenge for the durability of catalysts during the DRM is that the catalyst is prone to deactivation due to the carbon deposits produced by the thermodynamically inevitable side reactions ($2CO = CO_2 + C$, ΔH_{298} = –171 kJ mol^{-1}, $CH_4 = 2\,H_2 + C$, ΔH_{298} = 75 kJ mol^{-1}). To investigate catalysts' endurance, the test of long-term photothermocatalytic DRM on Co/Mg-$CoAl_2O_4$ and Co/$CoAl_2O_4$ was performed. In Fig. 5A, Co/Mg-$CoAl_2O_4$ exhibits excellent photothermocatalytic durability. After the catalyst was reacted for 60 h, its r_{H2} and r_{CO} are slightly reduced by 7.83 % and 6.53 % compared to the initial 1 hour (Fig. 5A). The η value of Co/Mg-$CoAl_2O_4$ is still high up to 30 %. For Co/$CoAl_2O_4$, there are 3.1 %, and 10.7 % decrease for r_{H2}, and r_{CO} after only 17 h photothermocatalytic DRM reaction (Figure S5). Subsequently, to quantify the carbon deposition amount, the used Co/Mg-$CoAl_2O_4$ and Co/$CoAl_2O_4$ samples after long-term photothermocatalytic DRM were characterized by TG-MS, TEM and Raman. TG-MS analysis demonstrates that due to the combustion of sedimentary carbon, the weight loss rate of the used sample of Co/Mg-$CoAl_2O_4$ is 42.57 % after 60 h photothermocatalytic DRM reaction (Fig. 5B).

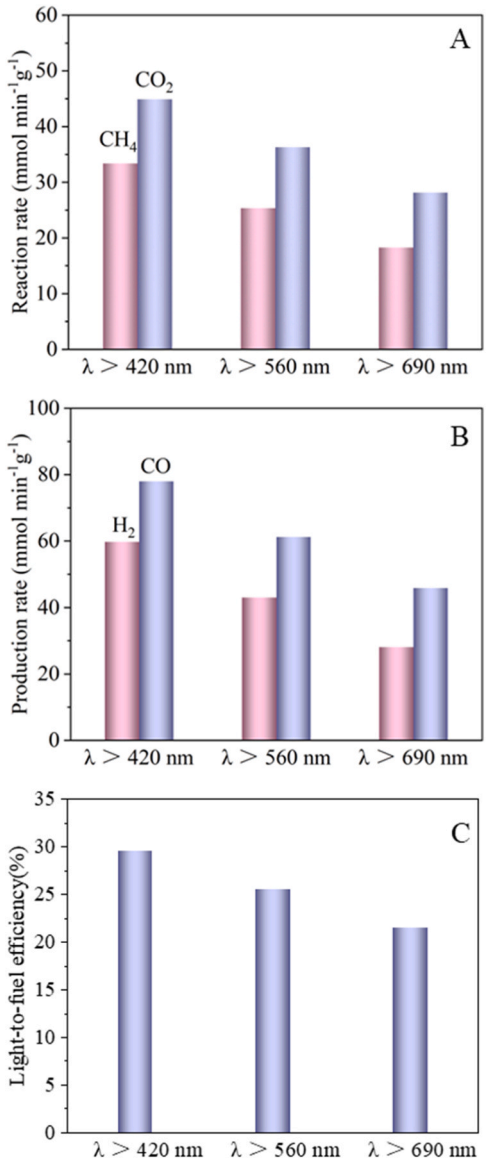

Fig. 4. The values of r_{CH4} and r_{CO2} (A), the values of r_{H2} and r_{CO} (B), and the values of η (C) of Co/Mg-$CoAl_2O_4$ for photothermocatalytic DRM with concentrated vis-IR irradiation.

Surprisingly, a weight loss rate of 84.46 % is observed for the used Co/$CoAl_2O_4$ sample after only 17 h photothermocatalytic DRM reaction (Fig. 5C). Following the results of the weight loss rate, the carbon deposition rate (r_C) of Co/Mg-$CoAl_2O_4$ is calculated quite low (0.0124 g_c h^{-1} $g^{-1}_{catalyst}$), only 0.038 times of that Co/$CoAl_2O_4$ (r_C = 0.3197 g_c h^{-1} $g^{-1}_{catalyst}$) (Fig. 5D). TEM images verify that a large number of carbon nanotubes are in the Co/Mg-$CoAl_2O_4$ and Co/$CoAl_2O_4$ samples (Figures S6 and S7). HRTEM image of the used Co/Mg-$CoAl_2O_4$ sample reveals that though surrounded by carbon, a visible lattice spacing of (111) facets of Co nanoparticle still be detected (Figure S6). However, for the used Co/$CoAl_2O_4$ sample, the surface of the Co nanoparticle is blurred for being covered by carbon (Figure S7). Raman results show that both the catalysts after the photothermocatalytic DRM reaction have strong Raman peaks of carbon (Figure S8), which were consistent with TG-MS and TEM results, confirming the formation of coke.

3.4. Reasons for enhanced photothermocatalytic activity and anti-coking performance

3.4.1. CO_2 adsorption capacity

Reaction steps of CO_2 adsorption, activation, and dissociation are essential in DRM, and the products following the reactions will be further reacted with carbon species generated by the dissociation of CH_4. To explore why Co/Mg-$CoAl_2O_4$ has an improvement in photothermocatalytic activity and excellent resistance to coking compared to Co/$CoAl_2O_4$, we conducted experiments on the CO_2 adsorption capacity of Co/$CoAl_2O_4$ and Co/Mg-$CoAl_2O_4$. The CO_2 adsorption isotherm of Co/Mg-$CoAl_2O_4$ is higher than that of Co/$CoAl_2O_4$ at 0 °C (ice water) (Fig. 6A). According to the data shown in Fig. 6A, by plotting P/P_0 versus $1/[Q(P_0/P-1)]$, the monolayer saturation adsorption capacity (Q) of Co/$CoAl_2O_4$ and Co/Mg-$CoAl_2O_4$ was calculated (Fig. 6B). Both of them have a good linear relationship. The Q value for Co/Mg-$CoAl_2O_4$ is 2.79 cm^3 g^{-1} STP, superior to that of Co/$CoAl_2O_4$ (2.65 cm^3 g^{-1} STP). This reveals that Mg^{2+} doping in Co/Mg-$CoAl_2O_4$ promotes the CO_2 adsorption capacity of the catalyst.

3.4.2. CO_2-TPD

To further investigate the adsorption capacity of CO_2 on samples, we performed the temperature-programmed CO_2 desorption (CO_2-TPD) on Co/Mg-$CoAl_2O_4$ and Co/$CoAl_2O_4$ in the dark. As shown in Fig. 7, a broader CO_2 desorption peak of Co/$CoAl_2O_4$ at about 92 °C was recorded, mainly due to the desorption of CO_2 adsorbed on the sample surface. For Co/Mg-$CoAl_2O_4$, the desorption peak of CO_2 appears at a higher temperature (around 98 °C) and the intensity of the desorption peak is significantly higher than that of Co/$CoAl_2O_4$. This indicates that the Mg^{2+} doping greatly strengthens the adsorption capacity of CO_2, thus resulting in more CO_2 participating in the oxidation of carbon species.

3.4.3. Isotope labeling of $^{12}C^{18}O_2$

To explore the other determinant of the improved anti-coking performance of Co/Mg-$CoAl_2O_4$, we performed the isotope labeling experiment in the $^{12}CH_4$ photothermocatalytic reduction of $^{12}C^{18}O_2$ on Co/Mg-$CoAl_2O_4$ under focused UV–vis–IR irradiation. The peaks at 2324 and 2309 cm^{-1} belong to the C–O stretching peaks of $^{12}C^{18}O_2$ before the reaction begins (Fig. 8A). After 20 mins of photothermocatalytic DRM, the peaks at 2131 and 2082 cm^{-1} belong to C–O stretching of $^{12}C^{18}O$ and the peaks at 2165 and 2114 cm^{-1} belong to C–O stretching of $^{12}C^{16}O$ are observed. The production of $^{12}C^{16}O$ reveals the O atoms of Co–O bonds in $CoAl_2O_4$ participating in the oxidation of carbon species, which is generated by CO disproportionation and CH_4 dissociation. The peaks of C–O stretching at 2324 and 2343 cm^{-1} belonging to $^{12}C^{16}O^{18}O$, suggests the further oxidation of $^{12}C^{18}O$ by O atoms in $CoAl_2O_4$ and/or $^{12}C^{16}O$ by ^{18}O (produced by $^{12}C^{18}O_2$ dissociation). This contributes to the reduction of the carbon deposition rate, consequently improving the coking resistance of the catalysts. Raman spectroscopy was applied to further investigate on the used sample of Co/Mg-$CoAl_2O_4$ after the isotope labeling experiment. The result shows a Raman peak at 666 cm^{-1} (Fig. 8B). Compared to the stretching peak of Co–^{16}O at 656 cm^{-1} in a fresh Co/Mg-$CoAl_2O_4$ sample (Fig. 8B), the significant isotope shift implies the transformation from Co–^{16}O bonds to Co–^{18}O bonds in $CoAl_2O_4$. This result unveils that O atoms of Co–O bonds in $CoAl_2O_4$ exactly engages in the C* oxidation.

3.4.4. light absorption capacity

The ultraviolet-visible diffuse reflectance spectroscopy was carried out to explore the optical properties of the samples. Mg-$CoAl_2O_4$ and Co/$CoAl_2O_4$ have strong light absorption. Co/Mg-$CoAl_2O_4$ also has the stronger peaks of absorption spread across the entire solar spectrum, which is attributed to the strong surface plasmon absorption of Co nanoparticles and the strong optical absorption of Mg-$CoAl_2O_4$, and the optical absorption is significantly amplified by the near-field dielectric

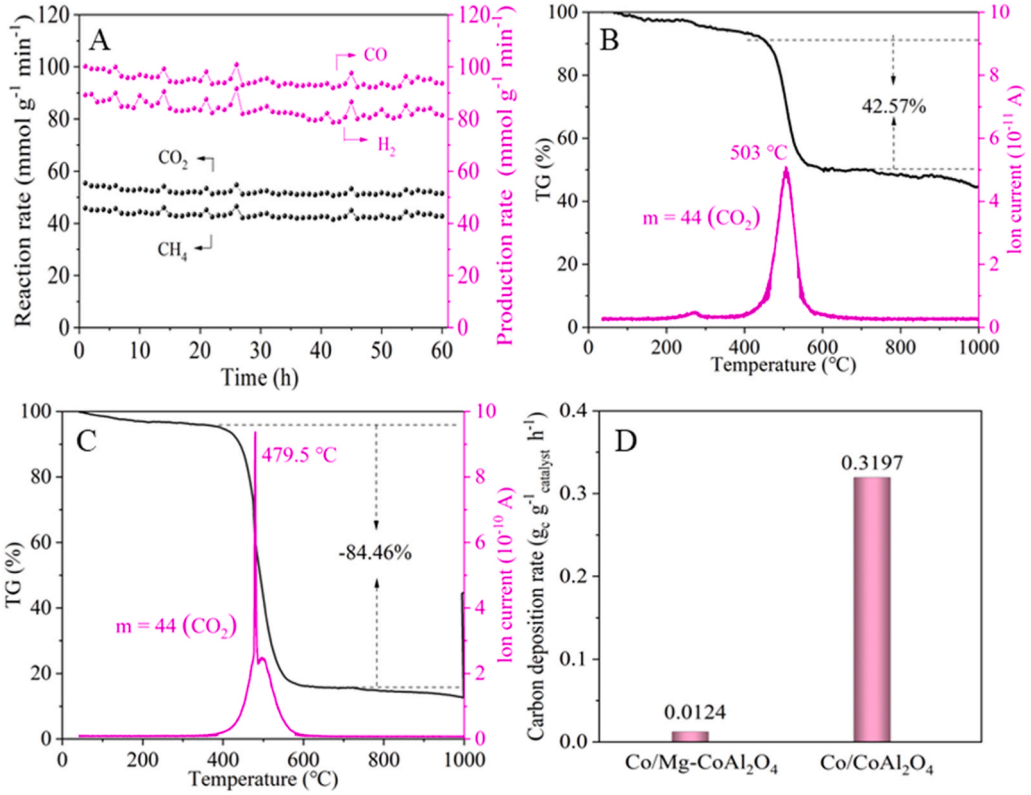

Fig. 5. Reaction and production rates on Co/Mg-$CoAl_2O_4$ under focused UV–vis–IR irradiation during 60 h photothermocatalytic DRM reaction (A). TG-MS profiles of the used catalysts of Co/Mg-$CoAl_2O_4$ (B) after 60 h photothermocatalytic DRM reaction and of Co/$CoAl_2O_4$ (C) after 17 h photothermocatalytic DRM reaction. The carbon deposition rates of Co/Mg-$CoAl_2O_4$ and Co/$CoAl_2O_4$ during the photothermocatalytic DRM tests (D).

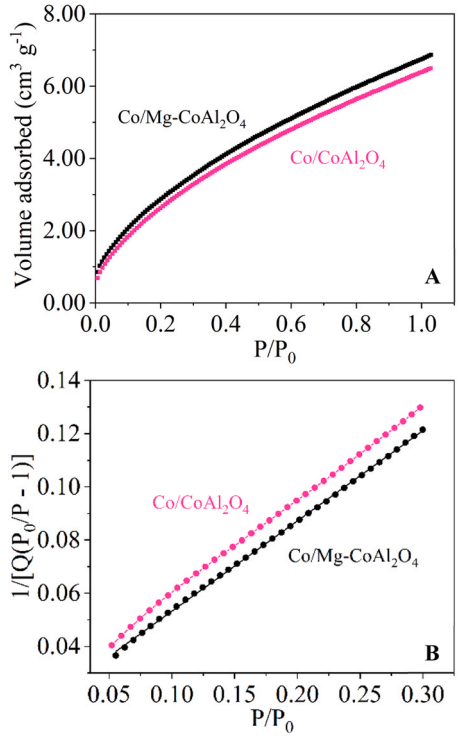

Fig. 6. CO_2 adsorption isotherms (A). The profiles of P/P_0 vs $1/[Q(P_0/P\text{-}1)]$ (B) are based on their CO_2 adsorption isotherms at 0 °C.

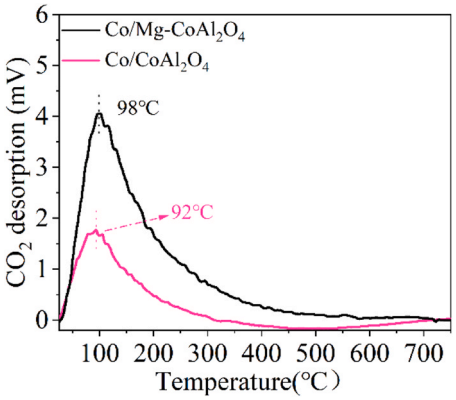

Fig. 7. CO_2-TPD profiles of Co/Mg-$CoAl_2O_4$ and Co/$CoAl_2O_4$ in the dark.

scattering effect of the carrier [37] (Fig. 10A).

On the basis of CO_2 adsorption capacity, isotope labeling experiment on Co/Mg-$CoAl_2O_4$, and the light absorption capacity of Co/Mg-$CoAl_2O_4$, the intrinsic reasons of gaining better coking resistance are the synergetic effect between Mg^{2+} doping, active lattice oxygen and strong light absorption of Mg-$CoAl_2O_4$.This synergetic effect can be elucidated as depicted in Fig. 9. Due to the strong light absorption of Co/Mg-$CoAl_2O_4$, the photothermocatalytic DRM starts at a lower light intensity. CH_4 is dissociated on metallic Co nanoparticles to C* and H*, CO* and O* are dissociated from CO_2, and then C* is oxidized to CO* by O*. Meanwhile, several CO_2 are attached to Mg^{2+} doped on $CoAl_2O_4$ owing to the strong CO_2 adsorption property of Mg^{2+}. Subsequently, the part of carbon species are oxidized by adsorbed CO_2, while another part of carbon species via the interface migrate to $CoAl_2O_4$ and are oxidized from O atoms of Co–O bonds in $CoAl_2O_4$. The oxygen vacancies left on

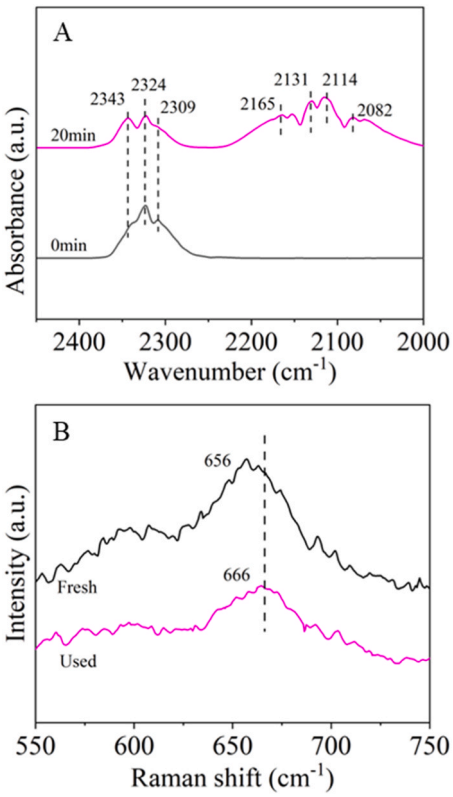

Fig. 8. The evolution of FTIR spectra in reduction of $^{12}C^{18}O_2$ by $^{12}CH_4$ on Co/Mg-$CoAl_2O_4$ under focused UV-Vis-IR illumination time (A). Raman spectra of fresh Co/Mg-$CoAl_2O_4$ sample and the used Co/Mg-$CoAl_2O_4$ sample after the isotope labeling test (B).

$CoAl_2O_4$ is reoccupied by the O atoms from CO_2 dissociation and simultaneously producing CO. This process not only significantly accelerates the C* oxidation, resulting in a significant increase in catalyst activity, but also effectively improves the catalysts' resistance to coking by hindering the polymerization of deposited carbon. Thus, Co/Mg-$CoAl_2O_4$ possesses excellent photothermocatalytic performance at a relative low light intensity.

3.5. Roles of light

3.5.1. Photothermocatalytic DRM

Co/Mg-$CoAl_2O_4$ is proven to have strong light absorption ability (Fig. 10A). As Co/Mg-$CoAl_2O_4$ is not a semiconductor, and it shows no activity in photocatalytic DRM at room temperature (Fig. 10B), the high photothermocatalytic DRM activity on Co/Mg-$CoAl_2O_4$ derives from a light-driven thermocatalysis. Due to the strong absorption of Co/Mg-$CoAl_2O_4$ and IR heating of light, the surface temperature of Co/Mg-$CoAl_2O_4$ ascends swiftly and enters into an equilibrium in a short time (Figure S9). In case the equilibrium temperature (T_{eq}) surpasses the light-off temperature of DRM ($T_{light\text{-}off}$), reactants and products begin to generate. As proven by thermocatalytic DRM (Figs. 11A and 11B), the $T_{light\text{-}off}$ is 600 °C. The T_{eq} of Co/Mg-$CoAl_2O_4$ with focused UV–vis–IR illumination and focused vis-IR illumination were recorded. Due to the infrared heating effect of illumination, the sample holder has a T_{eq} of 542 °C. Due to the intense optical absorption, the T_{eq} of Co/Mg-$CoAl_2O_4$ reaches 695 °C, well overpassing the $T_{light\text{-}off}$. Then, the efficient light-driven thermocatalytic DRM occurs, leading to high photo-thermocatalytic DRM activity.

3.5.2. Photoactivation

To examine the roles of light besides working as a heating source in photothermocatalytic DRM on Co/Mg-$CoAl_2O_4$, we performed catalytic DRM tests on Co/Mg-$CoAl_2O_4$ in the dark and with focused illumination at various temperatures. Thermocatalytic DRM in the dark condition was initiated when the temperature reached 600 °C (Figs. 11A and 11B). At the same temperature over 600 °C, the r_{CO2} and r_{CH4} exhibit a

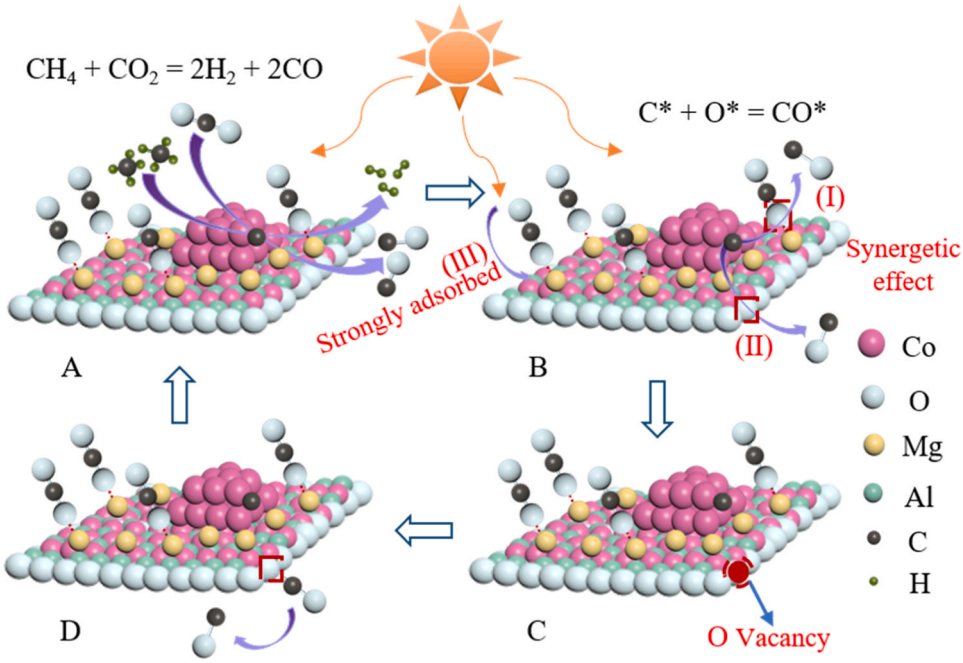

Fig. 9. Schematic diagram of synergetic effect on Co/Mg-$CoAl_2O_4$: strong light absorption Co/Mg-$CoAl_2O_4$ resulting in efficiently light-promoted DRM on Co nanoparticles (A), two processes (I and II) that inhibit carbon deposition: adsorbed CO_2 on doped Mg^{2+} reacts with carbon species on Co nanoparticles at the interface to form CO (B), active O atoms in $CoAl_2O_4$ are engaged in the C* oxidation (B), generating oxygen vacancies (C), and CO_2 adsorbed on the oxygen vacancies is converted to CO (D).

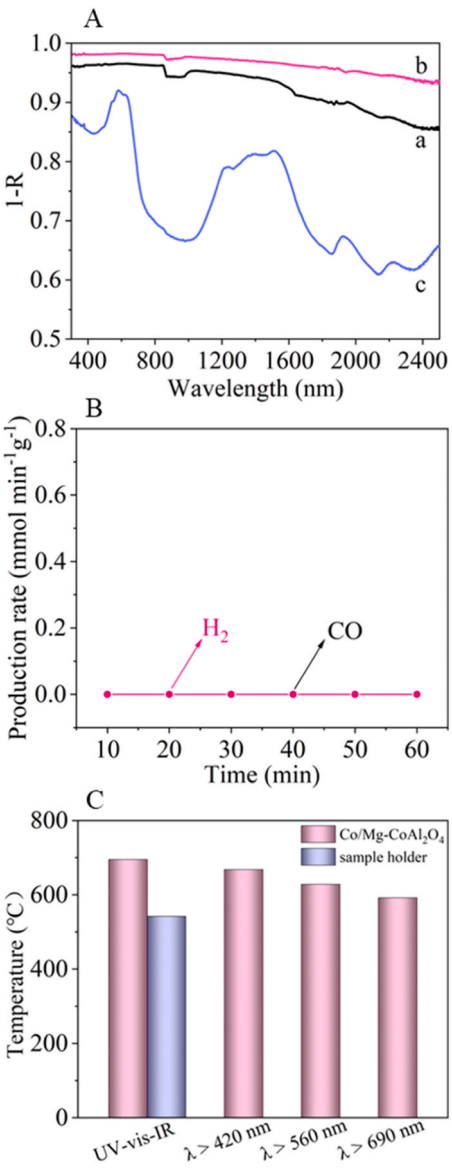

Fig. 10. Absorption spectra of Co/Mg-$CoAl_2O_4$ (a), Co/$CoAl_2O_4$ (b), Mg-$CoAl_2O_4$ (c) (R is reflectance) (A), photocatalytic DRM on Co/Mg-$CoAl_2O_4$ at room temperature (B). The T_{eq} values of Co/Mg-$CoAl_2O_4$ and sample holder with focused vis-IR illumination (C).

noticeable enhancement under concentrated UV–vis–IR irradiation contrasted with those in the dark. Great improvement of light-induced catalytic activities is also found with concentrated vis-IR illumination filtered by 420 and 560 nm filters (Fig. 11A and B). Meanwhile, the ratio of H_2 to CO also increases with concentrated vis-IR illumination at the same temperature in contrast to those in the dark (Fig. 11C). The significant improvement in the catalytic activity of photothermocatalytic DRM on Co/Mg-$CoAl_2O_4$ reveals that light evokes a photoactivation effect in addition to act as a heat source. For the deep detection of photoactivation, the evolution of $\ln(r_{CH4})$ with $1/T$ was plotted based on the r_{CH4} of the samples at different temperatures. As shown in Fig. 11D, a well-linear relationship is observed among $\ln(r_{CH4})$ and $1/T$. The value of apparent activation energy ($E_{a,\ ap}$) for Co/Mg-$CoAl_2O_4$ under focused UV–vis–IR irradiation is evaluated at 72.42 kJ mol^{-1} depending on the Arrhenius equation ($k = Ae^{-Ea/RT}$). Similarly, their $E_{a,ap}$ values are 110.59 and 112.57 kJ mol^{-1} under concentrated vis-IR irradiation filtered by 420 and 560 nm filters, respectively. Noteworthy, the activation energy in the dark is evaluated at 136.02 kJ mol^{-1}, far higher than the apparent activation energy under focused UV–vis–IR irradiation. The results profoundly reveal the significant contribution of light in reducing the $E_{a,ap}$, which leads to a remarkable enhancement of the photothermocatalytic activity.

It is known that DRM involves many basic steps including stepwise dissociation of CH_4, dissociation of CO_2 and oxidation of carbon species. Among these, the oxidation of carbon species is a determinative process as it requires the highest activation energy [34,42]. To further explore the photoactivation effect on Co/Mg-$CoAl_2O_4$ in DRM, we performed pre-adsorption of CO_2 temperature-programmed CH_4 oxidation (CH_4-TPO-CO_2) on Co/Mg-$CoAl_2O_4$ and Co/$CoAl_2O_4$ in the dark or with concentrated UV–vis–IR illumination conditions to investigate the effect of light. No obvious peak is observed on Co/Mg-$CoAl_2O_4$ in the dark condition even at a high temperature of 725 °C (Fig. 12A). In contrast, with focused UV–vis–IR illumination, two visible peaks at 2171 and 2114 cm^{-1} come into existence at 550 °C, which belong to the C–O stretching peaks of CO, and the peaks enhance with increasing temperature (Fig. 12B). The result suggests that the focused UV–vis–IR illumination is conducive to the oxidation of carbon species. As to Co/$CoAl_2O_4$, no peaks of CO are detected despite the temperature being raised to 725 °C in the dark condition (Fig. 12C). But under UV–vis–IR irradiation, the weak CO peaks appear at the temperature up to 700 °C (Fig. 12D), 150 °C later than the temperature those of Co/Mg-$CoAl_2O_4$. This implies that light accelerates the reaction between the absorbed CO_2 on MgO and the carbon species. For Co/Mg-$CoAl_2O_4$, the photoactivation effect greatly promotes the oxidation of carbon species and accelerates the reaction between the absorbed CO_2 on Mg^{2+} doped $CoAl_2O_4$ and the carbon species. These not only improve the photothermocatalytic activity of the catalyst but also enhance the coking resistance, further enabling Co/Mg-$CoAl_2O_4$ to achieve good photothermocatalytic performance at a lower light intensity,

4. Conclusions

In this work, a nanostructure of metallic Co nanoparticles loaded on Mg-doped $CoAl_2O_4$ (Co/Mg-$CoAl_2O_4$) was designed. Co/Mg-$CoAl_2O_4$ possesses extremely high photothermocatalytic DRM activity and stability at a low intensity of focused light. The high photothermocatalytic activity and improved coking resistance are attributed to the synergetic effect between Mg^{2+} doping, active lattice oxygen and strong light absorption of Mg-$CoAl_2O_4$. The enhanced CO_2 adsorption capacity by Mg^{2+} doping causes more CO_2 reacting with deposited carbon, and the active O atoms in $CoAl_2O_4$ being engaged in the C* oxidation. The strong light absorption of Mg-$CoAl_2O_4$ leads to strong light absorption capacity of Co/Mg-$CoAl_2O_4$, thus Co/Mg-$CoAl_2O_4$ can realize high photothermocatalytic activity at even low light intensity. The efficient photothermocatalytic DRM arises from photothermocatalysis. Photoactivation is evidenced to dramatically decrease activation energy and promote the C* oxidation, greatly strengthening the photothermocatalytic activity. Light also accelerates absorbed CO_2 reacting with C* under focused illumination, and the rapid C* oxidation hinders the polymerization of deposited carbon. This work helps realize highly efficient solar fuel production at relatively low intensity and designs Co-based catalysts with improved coking resistance.

CRediT authorship contribution statement

Zhengyan Cui: Writing – original draft, Methodology, Investigation, Conceptualization. **Qianqian Hu:** Writing – review & editing, Writing – original draft, Methodology, Investigation. **Yuanzhi Li:** Writing – original draft, Methodology, Funding acquisition, Conceptualization. **Jichun Wu:** Writing – review & editing, Methodology. **Mengqi Zhong:** Writing – review & editing, Methodology. **Zhi Chen:** Writing – review & editing, Methodology. **Lei Ji:** Writing – review & editing, Methodology. **Xiaocui Yu:** Writing – review & editing, Methodology. **Huamin Cao:** Writing – review & editing, Methodology.

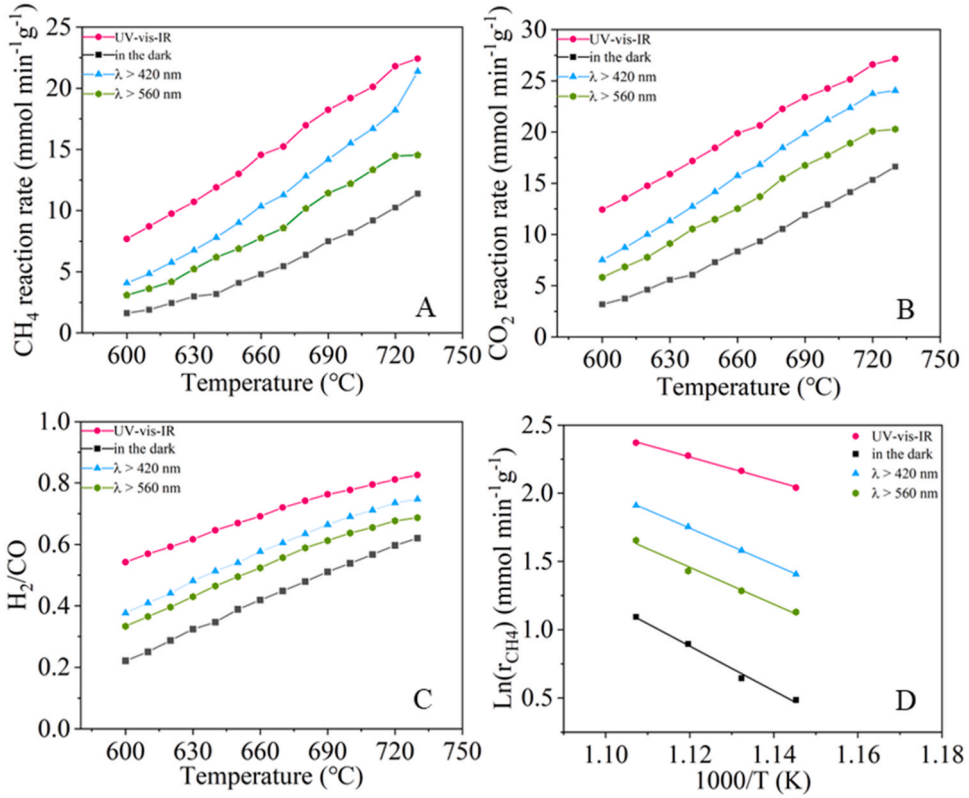

Fig. 11. Temperature-dependent r_{CH4} (A) and r_{CO2} (B), H_2/CO (C) and the corresponding plot of ln(r_{CH4}) with 1/T (D) for catalytic DRM on Co/Mg-$CoAl_2O_4$ with or without focused light condition.

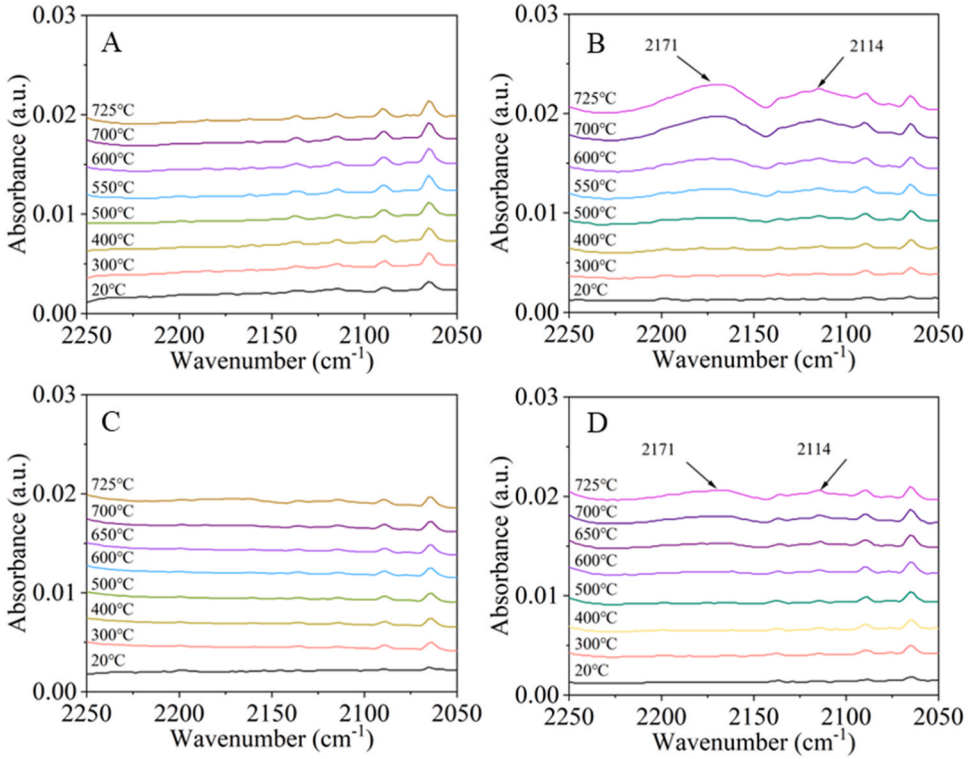

Fig. 12. FTIR spectra of the outcomes for temperature-programmed CH_4 oxidation by pre-adsorbed CO_2 on Co/Mg-$CoAl_2O_4$: in the dark (A), under focused illumination (B), and on Co/$CoAl_2O_4$: in the dark (C), under focused illumination (D).

Declaration of Competing Interest

The authors declare that they have no known competing financial interests or personal relationships that could have appeared to influence the work reported in this paper.

Data availability

Data will be made available on request.

Acknowledgments

This work was supported by the National Natural Science Foundation of China (21972109, 21673168).

Appendix A. Supporting information

Supplementary data associated with this article can be found in the online version at doi:10.1016/j.apcatb.2024.123917.

References

[1] M. Wei, C.A. McMillan, S. de la Rue du Can, Electrification of industry: potential, challenges and outlook, Curr. Sustain. Renew. Energy Rep. 6 (2019) 140–148, https://doi.org/10.1007/s40518-019-00136-1.
[2] W.L. Gao, S.Y. Liang, R.J. Wang, Q. Jiang, Y. Zhang, Q.W. Zheng, B.Q. Xie, C. Y. Toe, X.C. Zhu, J.Y. Wang, L. Huang, Y.S. Gao, Z. Wang, C. Jo, Q. Wang, L. D. Wang, Y.F. Liu, B. Louis, J. Scott, A. Roger, R. Amal, H. He, S.E. Park, Industrial carbon dioxide capture and utilization: state of the art and future challenges, Chem. Soc. Rev. 49 (2020) 8584–8686, https://doi.org/10.1039/d0cs00025f.
[3] A.M. Alhassan, I. Hussain, O.A. Taialla, M.M. Awad, A. Tanimu, K. Alhooshani, S. A. Ganiyu, Advances in catalytic dry reforming of methane (DRM): emerging trends, current challenges, and future perspectives, J. Clean. Prod. 423 (2023) 138638, https://doi.org/10.1016/j.jclepro.2023.138638.
[4] J.Y. Yan, C.H. Wang, H. Ma, Y.Y. Li (Dr), Y.C. Liu, N. Suzuki, C. Terashima, A. Fujishima, X.T. Zhang, Photothermal synergic enhancement of direct Z-scheme behavior of $Bi_4TaO_8Cl/W_{18}O_{49}$ heterostructure for CO_2 reduction, Appl. Catal. B-Environ. 268 (2020) 118401, https://doi.org/10.1016/j.apcatb.2019.118401.
[5] H. Bian, T.F. Liu, D. Li, Z. Xu, J.H. Lian, M. Chen, J.Q. Yan, S.Z. Frank Liu, Unveiling the effect of interstitial dopants on CO_2 activation over $CsPbBr_3$ catalyst for efficient photothermal CO_2 reduction, Chem. Eng. J. 435 (2022) 135071, https://doi.org/10.1016/j.cej.2022.135071.
[6] S.M. Li, C.H. Wang, D.S. Li, Y.M. Xing, X.T. Zhang, Y.C. Liu, Bi_4TaO_8Cl/Bi heterojunction enables high-selectivity photothermal catalytic conversion of CO_2-H_2O flow to liquid alcohol, Chem. Eng. J. 435 (2022) 135133, https://doi.org/10.1016/j.cej.2022.135133.
[7] S. Joo, K. Kim, O. Kwon, J. Oh, H.J. Kim, L.J. Zhang, J. Zhou, J.Q. Wang, H. Y. Jeong, J.W. Han, G. Kim, Enhancing thermocatalytic activities by upshifting the d-band center of exsolved Co-Ni-Fe ternary alloy nanoparticles for the dry reforming of methane, Angew. Chem. Int. Ed. 60 (2021) 15912–15919, https://doi.org/10.1002/anie.202101335.
[8] X.Y. Li, C. Wang, J.W. Tang, Methane transformation by photocatalysis, Nat. Rev. Mater. 7 (2022) 617–632, https://doi.org/10.1038/s41578-022-00422-3.
[9] E. Yang, E. Nam, Y. Jo, K. An, Coke resistant $NiCo/CeO_2$ catalysts for dry reforming of methane derived from core@shell Ni@Co nanoparticles, Appl. Catal. B-Environ. 339 (2023) 123152, https://doi.org/10.1016/j.apcatb.2023.123152.
[10] Z. Li, J. Leng, H. Yan, D.P. Zhang, D.L. Ren, F.L. Li, Y.B. Liu, X.B. Chen, C.H. Yang, Enhanced activity and stability for combined steam and CO_2 reforming of methane over $NiLa/MgAl_2O_4$ catalyst, Appl. Surf. Sci. 638 (2023) 158059, https://doi.org/10.1016/j.apsusc.2023.158059.
[11] J. Deng, K.K. Bu, Y.J. Shen, X.Y. Zhang, J.P. Zhang, K. Faungnawakij, D.S. Zhang, Cooperatively enhanced coking resistance via boron nitride coating over Ni-based catalysts for dry reforming of methane, Appl. Catal. B-Environ. 302 (2022) 120859, https://doi.org/10.1016/j.apcatb.2021.120859.
[12] K. Feng, S.R. Qian, Z.H. Zhang, Z.W. Li, X.H. Sun, Y. Cheng, B.H. Yan, Functionalization of inert silica to construct Si-O-Ni interfacial sites for stable dry reforming of methane, Chem. Eng. J. 465 (2023) 142808, https://doi.org/10.1016/j.cej.2023.142808.
[13] Y.F. Huang, D. Wei, Z.Y. Li, Y. Mao, Y.Q. Huang, B. Jin, X. Luo, Z.W. Liang, A highly efficient and stable TiO_2@NH_2-MIL-125 material for enhanced photocatalytic conversion of CO_2 and CH_4, Sep. Purif. Technol. 310 (2023) 123174, https://doi.org/10.1016/j.seppur.2023.123174.
[14] J. Yang, J. Wang, W.J. Zhao, G.H. Wang, K. Wang, X.H. Wu, J.M. Li, 0D/1D $Cu_{2-x}S$/TiO_2 S-scheme heterojunction with enhanced photocatalytic CO_2 reduction performance via surface plasmon resonance induced photothermal effects, Appl. Surf. Sci. 613 (2023) 156083, https://doi.org/10.1016/j.apsusc.2022.156083.
[15] Q.Y. Lin, J.W. Zhao, P. Zhang, S. Wang, Y. Wang, Z.Z. Zhang, N. Wen, Z.X. Ding, R. S. Yuan, X.X. Wang, J.L. Long, Highly selective photocatalytic reduction of CO_2 to CH_4 on electron-rich Fe species cocatalyst under visible light irradiation, Carbon Energy (2024) e435, https://doi.org/10.1002/cey2.435.
[16] A. Tavasoli, M. Preston, G. Ozin, Photocatalytic dry reforming: what is it good for? Energy Environ. Sci. 14 (2021) 3098, https://doi.org/10.1039/d0ee02809f.
[17] L. Luo, L. Fu, H.F. Liu, Y.X. Xu, J.L. Xing, C.R. Chang, D.Y. Yang, J.W. Tang, Synergy of Pd atoms and oxygen vacancies on In_2O_3 for methane conversion under visible light, Nat. Commun. 13 (2022) 2930, https://doi.org/10.1038/s41467-022-30434-0.
[18] W.K. Xu, G.R. Zhang, J.S. Wang, H. Yu, W.W. Zhang, L.L. Shen, D.H. Mei, Enhanced intermolecular electron transfer in fluorinated metal-organic framework photocatalysts for efficient CO_2 reduction, Adv. Funct. Mater. (2023) 2312691, https://doi.org/10.1002/adfm.202312691.
[19] X.T. Wang, Z.Z. Wang, Y. Li, J.T. Wang, G.K. Zhang, Efficient photocatalytic CO_2 conversion over 2D/2D Ni-doped $CsPbBr_3/Bi_3O_4Br$ Z-scheme heterojunction: critical role of Ni doping, boosted charge separation and mechanism study, Appl. Catal. B-Environ. 319 (2022) 121895, https://doi.org/10.1016/j.apcatb.2022.121895.
[20] Q.J. Zhi, J. Zhou, W.B. Liu, L. Gong, W.P. Liu, H.Y. Liu, K. Wang, J.Z. Jiang, Covalent microporous polymer nanosheets for efficient photocatalytic CO_2 conversion with H_2O, Small 18 (2022) 2201314, https://doi.org/10.1002/smll.202201314.
[21] H. Zhang, J.M. Ma, S.Y. Wang, J.X. Ji, Z.C. Zeng, Z.R. Shen, Y.P. Du, C.H. Yan, Novel cerium-based sulfide nano-photocatalyst for highly efficient CO_2 reduction, Small 18 (2022) 2201332, https://doi.org/10.1002/smll.202201332.
[22] T.S. Zhang, Y.T. Zheng, X. Zhao, M.X. Lin, B.X. Yang, J.W. Yan, Z.Y. Zhuang, Y. Yu, Scalable synthesis of holey deficient 2D Co/NiO single-crystal nanomeshes via topological transformation for efficient photocatalytic CO_2 reduction, Small 19 (2023) 2206873, https://doi.org/10.1002/smll.202206873.
[23] S.J. Wan, J.S. Xu, S.W. Cao, J.G. Yu, Promoting intramolecular charge transfer of graphitic carbon nitride by donor-acceptor modulation for visible-light photocatalytic H_2 evolution, Interdiscip. Mater. 1 (2022) 294–308, https://doi.org/10.1002/idm2.12024.
[24] Y. Ding, S. Maitra, C.H. Wang, S. Halder, R.T. Zheng, T. Barakat, S. Roy, L.H. Chen, B.L. Su, Vacancy defect engineering in semiconductors for solar light-driven environmental remediation and sustainable energy production, Interdiscip. Mater. 1 (2022) 213–255, https://doi.org/10.1002/idm2.12025.
[25] E. Gong, S. Ali, C.B. Hiragond, H.S. Kim, N.S. Powar, D. Kim, H. Kim, S. In, Solar fuels: research and development strategies to accelerate photocatalytic CO_2 conversion into hydrocarbon fuels, Energy Environ. Sci. 15 (2022) 880–937, https://doi.org/10.1039/d1ee02714j.
[26] H.B. Yin, J.H. Li, New insight into photocatalytic CO_2 conversion with nearly 100 % CO selectivity by CuO-Pd/H_xMoO_{3-y} hybrids, Appl. Catal. B-Environ. 320 (2023) 121927, https://doi.org/10.1016/j.apcatb.2022.121927.
[27] D. An, S. Nishioka, S. Yasuda, T. Kanazawa, Y. Kamakura, T. Yokoi, S. Nozawa, K. Maeda, Alumina-supported alpha-iron(III) oxyhydroxide as a recyclable solid catalyst for CO_2 photoreduction under visible light, Angew. Chem. Int. Ed. 61 (2022) e202204948, https://doi.org/10.1002/anie.202204948.
[28] X. Cheng, J.M. Wang, K. Zhao, Y.P. Bi, Spatially confined iron single-atom and potassium ion in carbon nitride toward efficient CO_2 reduction, Appl. Catal. B-Environ. 316 (2022) 121643, https://doi.org/10.1016/j.apcatb.2022.121643.
[29] C.X. He, S.Q. Wu, L.Z. Wang, J.L. Zhang, Recent advances in photo-enhanced dry reforming of methane: A review, J. Photochem. Photobiol. C: Photochem. Rev. 51 (2022) 100468, https://doi.org/10.1016/j.jphotochemrev.2021.100468.
[30] S.W. Wu, Y.Z. Li, Q.Q. Hu, J.C. Wu, Q. Zhang, Photothermocatalytic dry reforming of methane for efficient CO_2 reduction and solar energy storage, ACS Sustain. Chem. Eng. 9 (2021) 11635–11651, https://doi.org/10.1021/acssuschemeng.1c03692.
[31] M. Cai, Z. Wu, Z. Li, L. Wang, W. Sun, A.A. Tountas, C. Li, S. Wang, K. Feng, A. B. Xu, S. Tang, A. Tavasoli, M. Peng, W. Liu, A.S. Helmy, L. He, G. Ozin, X. Zhang, Greenhouse-inspired supra-photothermal CO_2 catalysis, Nat. Energy 6 (2021) 807–814, https://doi.org/10.1038/s41560-021-00867-w.
[32] A. Zhang, S.W. Wu, Y.Y. Li, Q. Zhang, Q.Q. Hu, J.C. Wu, X. Tan, Y.D. Zhang, A novel synergetic effect between Ru and Cu nanoparticles for Ru-Cu/Al_2O_3 causes highly efficient photothermocatalytic CO_2 reduction with good durability, Appl. Surf. Sci. 556 (2021) 149821, https://doi.org/10.1016/j.apsusc.2021.149821.
[33] F.P. Pan, X.M. Xiang, Z.C. Du, E. Sarnello, T. Li, Y. Li, Integrating photocatalysis and thermocatalysis to enable efficient CO_2 reforming of methane on Pt supported CeO_2 with Zn doping and atomic layer deposited MgO overcoating, Appl. Catal. B-Environ. 260 (2020) 118189, https://doi.org/10.1016/j.apcatb.2019.118189.
[34] Q.Q. Hu, Y.Z. Li, J.C. Wu, Y.Q. Hu, H.M. Cao, Y. Yang, Extraordinary catalytic performance of nickel half-metal clusters for light-driven dry reforming of methane, Adv. Energy Mater. (2023) 2300071, https://doi.org/10.1002/aenm.202300071.
[35] Y. Chai, Y.H. Kong, M. Lin, W. Lin, J.N. Shen, J.L. Long, R.S. Yuan, W.X. Dai, X. X. Wang, Z.Z. Zhang, Metal to non-metal sites of metallic sulfides switching products from CO to CH_4 for photocatalytic CO_2 reduction, Nat. Commun. 14 (2023) 6168, https://doi.org/10.1038/s41467-023-41943-x.
[36] M.Y. Mao, Q. Zhang, Y. Yang, Y.Z. Li, H. Huang, Z.K. Jiang, Q.Q. Hu, X.J. Zhao, Solar-light-driven CO_2 reduction by methane on Pt nanocrystals partially embedded in mesoporous CeO_2 nanorods with high light-to-fuel efficiency, Green. Chem. 20 (2018) 2857, https://doi.org/10.1039/c8gc01058g.
[37] S.W. Wu, Y.Z. Li, Q. Zhang, Z.K. Jiang, Y. Yang, J.C. Wu, X.J. Zhao, High light-to-fuel efficiency and CO_2 reduction rates achieved on a unique nanocomposite of Co/Co-doped Al_2O_3 nanosheets with UV–vis–IR irradiation, Energy Environ. Sci. 12 (2019) 2581, https://doi.org/10.1039/c9ee01484e.

[38] Z.Y. Zhang, Q.Q. Hu, Y.Z. Li, Y.L. Chen, J.C. Wu, H.M. Cao, Effective UV–visible-infrared light-driven photothermocatalytic dry reforming of methane on Ni/Ni-MgO caused by a novel synergetic effect and photoactivation, Appl. Surf. Sci. 635 (2023) 157713, https://doi.org/10.1016/j.apsusc.2023.157713.

[39] X.L. Liu, Y.Y. Ling, C. Sun, H. Shi, H.B. Zheng, C. Song, K. Gao, C.Z. Dang, N. Sun, Y.M. Xuan, Y.L. Ding, Efficient solar-driven CO_2-to-fuel conversion via Ni/$MgAlO_x$@SiO_2, nanocomposites at low temperature, Fundam. Res. (2022) 2667–3258, https://doi.org/10.1016/j.fmre.2022.04.011.

[40] S.W. Wu, G.R. Ji, P. Qiu, Q.Q. Hu, J. Tian, Y.Z. Li, High Fuel Yields, Solar-to-Fuel Efficiency, and Excellent Durability Achieved for Confined NiCo Alloy Nanoparticles Using MgO Overlayers for Photothermocatalytic CO_2 Reduction, Sol. RRL 6 (2022) 2200369, https://doi.org/10.1002/solr.202200369.

[41] X.L. Liu, H. Shi, X.G. Meng, C. Sun, K. Zhang, L. Gao, Y. Ma, Z.K. Mu, Y.Y. Ling, B. Cheng, Y.L. Li, Y.M. Xuan, Y.L. Ding, Solar-enhanced CO_2 conversion with CH_4 over synergetic NiCo alloy catalysts with light-to-fuel efficiency of 33.8 %, Sol. RRL (2021) 2100185 https://doi.org/10.1002/solr.202100185.

[42] J.Q. Zhang, K. Xie, Y.C. Jiang, M. Li, X.J. Tan, Y. Yang, X.L. Zhao, L. Wang, Y. F. Wang, X.Y. Wang, Y.Z. Zhu, H.J. Chen, M.B. Wu, H.Q. Sun, S.B. Wang, Photoinducing different mechanisms on a Co-Ni bimetallic alloy in catalytic dry reforming of methane, ACS Catal. 13 (2023) 10855–10865, https://doi.org/10.1021/acscatal.3c02525.

[43] X.L. Liu, Z.K. Mu, C. Sun, H. Shi, X.G. Meng, P. Li, Y.Y. Li, B. Cheng, Y.M. Xuan, Y. L. Ding, Highly efficient solar-driven CO_2-to-fule conversion assisted by CH_4 over NiCo-ZIF derived catalysts, Fuel 310 (2022) 122441, https://doi.org/10.1016/j.fuel.2021.122441.

[44] Z.H. Xie, Y.Z. Li, Z.Y. Zhou, Q.Q. Hu, J.C. Wu, S.W. Wu, Significantly enhancing the solar fuel production rate and catalytic durability for photothermocatalytic CO_2 reduction by a synergetic effect between Pt and Co-doped Al_2O_3 nanosheets, J. Mater. Chem. A 10 (2022) 7099, https://doi.org/10.1039/d2ta00211f.

[45] H. Huang, M.Y. Mao, Q. Zhang, Y.Z. Li, J.L. Bai, Y. Yang, M. Zeng, X.J. Zhao, Solar-light-driven CO_2 reduction by CH_4 on silica-cluster modified Ni nanocrystals with a high solar-to-fuel efficiency and excellent durability, Adv. Energy Mater. (2018) 1702472, https://doi.org/10.1002/aenm.201702472.

[46] J.Q. Zhou, Y.F. Lia, L. Yu, Z.P. Li, D.F. Xie, Y.Y. Zhao, Y. Yu, Facile in situ fabrication of Cu_2O@Cu metal-semiconductor heterostructured nanorods for efficient visible-light driven CO_2 reduction, Chem. Eng. J. 385 (2020) 123940, https://doi.org/10.1016/j.cej.2019.123940.

[47] Y.H. Qi, L.Z. Song, S.X. Ouyang, X.C. Liang, S.B. Ning, Q.Q. Zhang, J.H. Ye, Photoinduced defect engineering: enhanced photothermal catalytic performance of 2D black In_2O_{3-x} nanosheets with bifunctional oxygen vacancies, Adv. Mater. 32 (2020) 1903915, https://doi.org/10.1002/adma.201903915.

[48] X. Chen, Q. Li, M. Zhang, J.J. Li, S.C. Cai, J. Chen, H.P. Jia, MOF-templated preparation of Highly Dispersed Co/Al_2O_3 composite as the photothermal catalyst with high solar-to-fuel efficiency for CO_2 methanation, ACS Appl. Mater. Interfaces 12 (2020) 39304–39317, https://doi.org/10.1021/acsami.0c11576.

[49] Z. Wang, Z. Yang, R. Fang, Y. Yan, J. Ran, L. Zhang, A State-of-the-art review on action mechanism of photothermal catalytic reduction of CO_2 in full solar spectrum, Chem. Eng. J. 429 (2022) 132322, https://doi.org/10.1016/j.cej.2021.132322.

[50] Z.Y. Zhang, T. Zhang, W.P. Liang, P.W. Bai, H.Y. Zheng, Y. Lei, Z. Hu, T. Xie, Promoted solar-driven dry reforming of methane with Pt/mesoporous-TiO_2 photo-thermal synergistic catalyst: performance and mechanism study, Energy Convers. Manag. 258 (2022) 115496, https://doi.org/10.1016/j.enconman.2022.115496.

[51] L. Yu, X. Ba, M. Qiu, Y.F. Li, L. Shuai, W. Zhang, Z.F. Ren, Y. Yu, Visible-light-driven CO_2 reduction coupled with water oxidation on Cl-doped Cu_2O Nanorods, Nano Energy 60 (2019) 576–582, https://doi.org/10.1016/j.nanoen.2019.03.083.

[52] M.J. Li, Z.X. Sun, Y.H. Hu, Thermo-photo coupled catalytic CO_2 reforming of methane: a review, Chem. Eng. J. 428 (2022) 131222, https://doi.org/10.1016/j.cej.2021.131222.

[53] H.M. Cao, Y.Z. Li, Q.Q. Hu, J.C. Wu, L. Ji, A novel strategy for dramatically improving catalytic performance for light-driven thermocatalytic CO_2 reduction with CH_4 on Ru/MgO: the CO_2 molecular fencing effect promoted by photoactivation, J. Mater. Chem. A 11 (2023) 19645–19655, https://doi.org/10.1039/d3ta04267g.

[54] X.Y. Yan, B.C. Lu, H. Dong, Q.B. Liu, Solar-promoted photo-thermal CH_4 reforming with CO_2 over Ni/CeO_2 catalyst: experimental and mechanism studies, Appl. Energy 348 (2023) 121549, https://doi.org/10.1016/j.apenergy.2023.121549.